This paper appears in IEEE Transactions on Haptics, 2020, DOI: 10.1109/TOH.2020.2970906

Impact of Kinematic Structure on the Force Displayability of Planar Passive Haptic Devices

Maciej Łącki, Brayden DeBoon, and Carlos Rossa

***Abstract*—Haptic devices containing passive actuators, such as controllable brakes or dampers, are an attractive alternative to their motor-driven counterparts due to intrinsic stability and improved impedance bandwidth. Passive actuators cannot generate energy and, therefore, the output force can only oppose the applied velocity. In the same way the kinematic structure of traditional manipulators is designed to maximize dexterity and manipulability, one must consider adapting the device topology to optimize force displayability when designing passive actuators.**

This paper introduces a set of metrics to evaluate and compare the performance of 2-degree-of-freedom serial and parallel passive haptic devices. These metrics consider the impact of the kinematic structure on the force displayability according to the directions of the device velocity and desired force. Applying these metrics to 9 manipulators revealed that: 1.) Serial manipulators can generate passive forces in all directions equally regardless of the link length ratio; 2.) The base link length of 5-bar parallel manipulators strongly influences passive force displayability; 3.) 5-bar parallel manipulators with the base link length of zero can generate the widest range of passive forces when all links have the same length. The novel performance metrics presented in this paper can aid in the design of 2-DOF passive haptic devices.

***Index Terms*—Passive Haptics Devices, Passive Actuators, Planar Device, Kinematic Structure, Force Displayability**

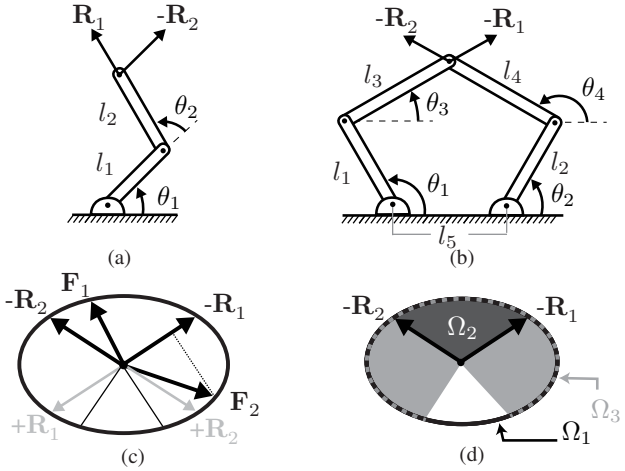

Fig. 1. Two types of manipulators: a serial RR shown in (a) and parallel five-bar mechanism shown in (b), showing the reference force directions $\mathbf{R}_1$ and $\mathbf{R}_2$. Based on the reference forces shown in (c) force $\mathbf{F}_1$ can be fully displayed, while $\mathbf{F}_2$ can be approximated using -$\mathbf{R}_1$. The force directions of the device, represented by Ω_1, are divided into regions shown in (d), where Ω_2 and Ω_3 represent the fully and partially displayable regions.

I. Introduction

INTERACTIONS with an ideal haptic interface must be indistinguishable from interactions with physical environments. Therefore, stability and transparency are paramount design considerations in any haptic device. Transparency requires a large impedance bandwidth while stability can only be maintained within a limited range [1]–[4]. Haptic devices with passive actuators in place of traditional electric motors are an alternative class of force feedback devices. Passivity of these devices guarantees stability, which in turn, allows them to generate high impedance without requiring high viscous damping. As a result, passive haptic devices can have a wider z-width than their active counterparts. These characteristics make passive haptic devices ideal for applications like robotic teleoperation, rehabilitation, or surgical simulation [5]–[8].

The nonlinearities introduced by the passivity of the brakes make passive devices difficult to control [6], [9]–[11]. Brakes can only generate forces or torques in the direction opposing their velocity. As a result, only the magnitude of the force of a passive device can be controlled, and not the direction [12]. This indicates that a passive haptic device cannot generate a force in an arbitrary direction [13]. The fundamental issue when designing a passive device is maximizing the force output capability, which may depend on its kinematic structure.

There are two main types of manipulator topologies: serial and parallel [3]. Serial manipulators, see Fig. 1(a), are composed of an open chain of actuated links. These manipulators have a larger workspace than their parallel counterparts with similar link lengths. Parallel manipulators, see Fig. 1(b), are formed by connecting two or more serial chains to a common end-effector. Distributing the load onto multiple links minimizes the relative motion of each actuator, resulting in lower apparent inertia of the device [3], [14], increased rigidity, and higher precision than in similar serial manipulators [14].

There are many tools available for examining performance of a manipulator. Condition number, used in [15], and global workspace condition number, proposed in [16], evaluate the accuracy of velocity and force output of a manipulator throughout its workspace. In [17] a unified framework for a holistic analysis of a manipulator, which is simultaneous analysis of acceleration, velocity, and force output capability, was developed using dynamic capability equations. Generalized manipulability ellipsoids, introduced in [18] and adapted for

Maciej Łącki, Brayden DeBoon, and Carlos Rossa are with Faculty of Engineering and Applied Science at Ontario Tech University, Oshawa, Ontario, Canada. E-mail: maciej.lacki@OntarioTechU.net, brayden.deboon@OntarioTechU.net, carlos.rossa@OntarioTechU.ca

We acknowledge the support of the Natural Sciences and Engineering Research Council of Canada (NSERC), [funding number 2018-06074]. Cette recherche a été financée par le Conseil de recherches en sciences naturelles et en génie du Canada (CRSNG), [numéro de référence 2018-06074].

parallel manipulators in [19], aid in visualizing and quantifying the ability of a manipulator to generate force in any direction. The ellipsoids were also used in [20] to determine the optimal pose for a redundant manipulator. The concept of ellipsoids was adopted for passive devices in [21], where passive manipulability ellipsoids were used to optimize a kinematically redundant planar 2-degree-of-freedom (DOF) parallel passive device.

The accuracy and the dynamic performance of serial and parallel manipulators was compared in [14] and [22], respectively. One unexplored issue is the impact of the kinematic structure on the force output capability of a passive device. We address this in this paper by developing a set of metrics measuring the output force capability of a generic passive haptic device. The novel metrics attempt to isolate the effects of actuator passivity by considering the percentage of the workspace where a desired force can be generate provided a velocity direction. These metrics complement the metrics for active devices such as [15]–[19] and unlike metrics proposed in [21], they provide a global overview of the performance changes due to change in velocity or desired force output directions. The metrics are evaluated on a subset of planar serial and parallel manipulators to demonstrate the impact of the kinematic structure on force displayability. We highlight significant differences and trade-offs to consider when choosing between serial and parallel structures for the design of a passive device.

To this end, Section II describes the force output of a passive haptic device. Based on this model a set of new performance metrics is derived in Section III and then used to evaluate 9 manipulators in Section IV. The results are then used to compare the performance of the manipulators in Section V, and conclude with a set of guidelines and recommendations for designing a 2-DOF passive haptic device in Section VI.

II. Modelling the Force Output of a Passive Haptic Device

An ideal n-DOF haptic device can output forces in arbitrary directions independent of current position and orientation of the end-effector $\mathbf{P} \in \mathbb{R}^{n\times 1}$, where $n \in \mathbb{N}$. However, the topology of the kinematic chain in haptic devices influences the direction and magnitude in which forces can be displayed. The kinematics of a device, represented by matrix $\mathbf{T}(\boldsymbol{\theta}) \in \mathbb{R}^{n\times 1}$ where $\mathbf{P} = \mathbf{T}(\boldsymbol{\theta})$, describe the end-effector position of a non-redundant n-DOF mechanism with respect to the joint angles $\boldsymbol{\theta} = [\theta_1 \ \theta_2 \ \cdots \ \theta_i]^{\mathrm{T}}$ and $i \in \mathbb{N}$ represents the number of non-redundant joints, therefore, for a fully-actuated device, i.e., $n = i$. Additionally, joint angular velocities $\dot{\boldsymbol{\theta}} = d\boldsymbol{\theta}/dt$ compute the Cartesian velocity of the end-effector $\mathbf{V} \in \mathbb{R}^{n\times 1}$ through the Jacobian $\mathbf{J} \in \mathbb{R}^{n\times n} \mid \mathbf{J} = \partial \mathbf{T}_j/\partial\theta_k$ by

$$\mathbf{V} = \mathbf{J}\,\dot{\boldsymbol{\theta}} \tag{1}$$

where $1 \leq j,k \leq n$. For a non-redundant manipulator, the Jacobian results in an $n \times n$ matrix. The forward kinematics determine the position of the end-effector for a given set of joint angles, while the inverse kinematics are used to find joint angles for a given end-effector position. For the 2-DOF serial manipulator, see Fig. 1(a), the Jacobian is:

$$\mathbf{J} = \begin{bmatrix} -l_2\,\sin(\theta_1+\theta_2) - l_1\,\sin\theta_1 & -l_2\,\sin(\theta_1+\theta_2) \\ l_2\,\cos(\theta_1+\theta_2) + l_1\,\cos\theta_1 & l_2\,\cos(\theta_1+\theta_2) \end{bmatrix} \tag{2}$$

[23] and the Jacobian of the parallel manipulator in Fig. 1(b) is [24]:

$$\mathbf{J} = \begin{bmatrix} \frac{l_1\,\sin(\theta_1-\theta_3)\,\sin(\theta_4)}{\sin(\theta_3-\theta_4)} & \frac{l_2\,\sin(\theta_4-\theta_2)\,\sin(\theta_3)}{\sin(\theta_3-\theta_4)} \\ -\frac{l_1\,\sin(\theta_1-\theta_3)\,\cos(\theta_4)}{\sin(\theta_3-\theta_4)} & -\frac{l_2\,\sin(\theta_4-\theta_2)\,\cos(\theta_3)}{\sin(\theta_3-\theta_4)} \end{bmatrix}. \tag{3}$$

The inverse transpose of the Jacobian relates the force in Cartesian space $\mathbf{F} \in \mathbb{R}^{n\times 1}$ experienced at the end-effector and joint torques $\boldsymbol{\tau} \in \mathbb{R}^{n\times 1} \mid \boldsymbol{\tau} = [\tau_1 \quad \tau_2 \quad \cdots \quad \tau_n]^{\mathrm{T}}$ such that

$$\mathbf{F} = \left(\mathbf{J}^{-1}\right)^{\mathrm{T}} \boldsymbol{\tau} \tag{4}$$

where each column of the inverse transpose Jacobian relates to a *reference force* at the end-effector i.e.,

$$(\mathbf{J}^{-1})^{\mathrm{T}} = \begin{bmatrix} R_{x_1} & R_{x_2} & \cdots & R_{x_n} \\ R_{y_1} & R_{y_2} & & R_{y_n} \\ \vdots & & \ddots & \vdots \\ \underbrace{R_{\gamma_1}}_{\mathbf{R}_1} & \underbrace{R_{\gamma_2}}_{\mathbf{R}_2} & \cdots & \underbrace{R_{\gamma_n}}_{\mathbf{R}_n} \end{bmatrix}. \tag{5}$$

Column 1 represents force vector $\mathbf{R}_1$ as shown in Fig. 1. Each column corresponds to a reference force $\mathbf{R}_j$ resulting from applying unit torque τ_j to a single joint j at a time. Summing the reference forces provides an overall output force $\mathbf{F}_a$ at the end-effector for a generic manipulator i.e.,

$$\mathbf{F}_a = \sum_{j=1}^{n} a_j\,\mathbf{R}_j \tag{6}$$

where $a_j \in \mathbb{R}$ represents scaling factors on each reference force. These scaling factors provide a convenient method of visualizing the forces that a passive device generates and they aid in approximating forces. Note that (6) and (4) are equivalent, thus, the torque $\tau_j = a_j$.

Consider Fig. 1(a) and (b), respectively demonstrating a dual-actuated serial manipulator and a five bar parallel manipulator, each with two controllable DOF. A combination of the reference forces -$\mathbf{R}_1$ and -$\mathbf{R}_2$ corresponds to the force resulting from negative torques $\tau_1 = -1, \tau_2 = 0$, and $\tau_1 = 0, \tau_2 = -1$, respectively. To generate force $\mathbf{F}_1$, shown in Fig. 1(c), a combination of both -$\mathbf{R}_1$ and -$\mathbf{R}_2$ must be used.

In an ideal device, $\forall\ (\mathbf{J}^{-1})^{\mathrm{T}} \in \mathbb{R}^{n\times n} \exists\ [a_1, a_2, \cdots a_n] \in \mathbb{R}$ such that $\mathbf{F}_a = \mathbf{F}_d$. In non-ideal devices, however, saturation exists in each actuator and therefore $\mid a_j \mid$ is bound to the maximum achievable torque τ_{max_j} of an actuator j. Introducing saturation to each actuator generates a range of possible output forces Ω_1 at the end-effector, as outlined in Fig. 1(d) where contour Ω_1 represents the maximum achievable force in any direction. This region enclosed by Ω_1 represents an arbitrary aggregation of the reference forces, which includes all forces the device can generate.

In the context of passive devices, the only forces that can be created must act against the angular velocity of the brake and in the direction of the reference force $\mathbf{R}_j$ i.e., $\dot{\theta}_j\,\tau_j < 0$. For devices with multiple passive actuators, the collaboration

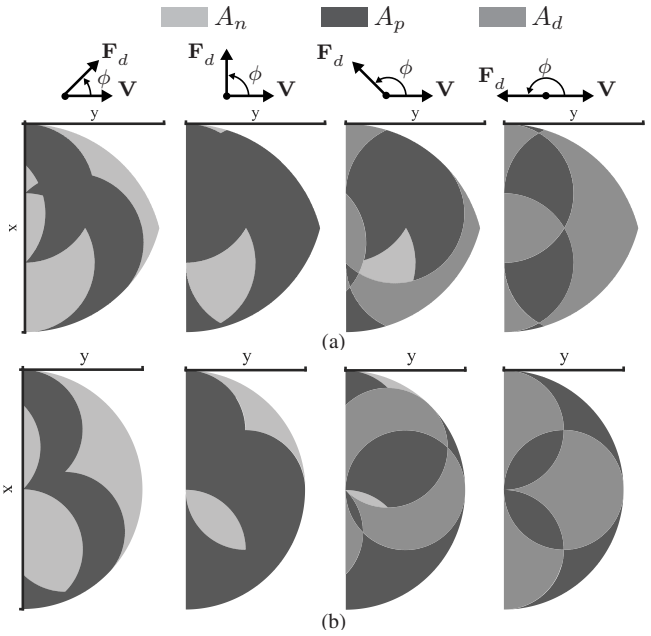

Fig. 2. The fully, partially, and non-displayable regions in workspace of parallel (a) and serial (b) passive devices for $\phi = \pi/4, \pi/2, 3\pi/4, \pi$, and $\alpha = \pi/2$. The parallel manipulator in (a) has link lengths $l_1 = l_2 = l_3 = l_4 = l_5 = 1$, and the serial manipulator in (b) has $l_1 = l_2 = 1$.

between each actuator can generate output forces in a direction that lies between the reference force of each actuator. As a result, the force output of a passive device becomes,

$$\mathbf{F}_a = \sum_{j=1}^{n} \beta_j \ \mathrm{sgn}(-\dot{\theta}_j)\, \mathbf{R}_j, \tag{7}$$

where $\beta_j \in \mathbb{R}\,[0 \quad \tau_{max_j}]$ represents the magnitude of the braking torque on an actuator n, and $\mathrm{sgn}(-\dot{\theta}_j)$ represents a nonlinear signum function which models the direction of the torque output of a moving brake [12]. This reduces the range of *fully displayable forces*; that is, the forces a passive device can accurately generate. The newly bounded range of displayable forces Ω_2 is a subset of Ω_1, as shown in Fig. 1(d), restricting the ability to render a desired force in various locations in the task-space. To mitigate this behaviour, the desired forces can be approximated through fractional combinations of the reference forces. Note that there are numerous methods of approximating the desired force [10], [11], [13]. Force approximation expands the range of forces a passive haptic device can create while sacrificing the precision of the force output. One of these methods, *partial force display* determines the regions in which components of an arbitrary desired force can be rendered [10], [11]. By projecting the desired force onto a displayable reference force, like $\mathbf{F}_2$ in Fig. 1(c), a component of the force can be displayed. This approximation is only achievable if the projection of the desired force onto the displayable reference force is greater than zero i.e., $\mathrm{sgn}(-\dot{\theta}_j)\, H(-\mathrm{sgn}(\dot{\theta}_j)\, \mathbf{R}_j \cdot \mathbf{F}_d)$, where $H()$ represents the Heaviside function. The *partially displayable* regions, defined as Ω_3, represent the forces that can be approximated using this method. This region is a subset of Ω_1, however, it always encompasses Ω_2, as in $\Omega_2 \subset \Omega_3 \subset \Omega_1$. The force output of the passive device including both fully and partially displayable forces is,

$$\mathbf{F}_a = \sum_{j=1}^{i} \beta_j \ D_j \ \mathrm{sgn}(-\dot{\theta}_j)\, \mathbf{R}_j, \tag{8}$$

where $D_j = \mathrm{sgn}(-\dot{\theta}_j)\, H(\mathrm{sgn}(-\dot{\theta}_j)\, \mathbf{R}_j \cdot \mathbf{F}_d)$ and $\mathbf{F}_a \simeq \mathbf{F}_d$. This approximated force is a function of the kinematics for a specific end-effector location which can provide insight on the local displayability of a force. Note that the reference forces change for every position in the entire workspace. To evaluate the performance of passive devices, it is necessary to expand the analysis to the workspace of the manipulators.

III. Performance Metrics for Passive Haptic Devices

To better understand the impact of the kinematic structure on force output capability of a passive haptic device one must isolate the effects of actuator passivity from the dynamics of the device. To this end, let us consider the area of the workspace where a given force can be either fully or partially-displayed as a performance metric.

The total workspace of a device A_t can be divided into 3 regions: A_d, A_p, and A_n, where subscript d, p and n correspond to fully, partially, and non-displayable regions, respectively, see Fig. 2. The displayability of the force at each point depends on directions of velocity and desired force. As shown in Fig. 3(a), the directions of the velocity are defined as an angle $\boldsymbol{\alpha}$ which for planar devices has one component, the angle from positive x axis, and for spatial devices two components, along x and y axes. The direction of the desired force is defined as an angle $\boldsymbol{\phi}$ separating velocity and the desired force along the same axes as $\boldsymbol{\alpha}$. Ideally, the device must be able to generate a force in any direction, for any velocity, everywhere in its workspace. A passive device, however, can only generate the desired force in some parts of its workspace.

The total workspace area of a device can be found by integrating all of the points in the workspace. Since the geometry of the workspace reassembles a circle, the total workspace area is found with a polar integral such that,

$$A = \int_0^{2\pi} \int_0^{\pi} \int_0^{1} r \, dr \, d\theta \, d\sigma \tag{9}$$

where $r = ||\mathbf{P}(r, \theta, \sigma)||$ is a point within the device's workspace, θ, σ, and r are the polar coordinates. The area of the region where a force can be fully displayed or approximated is found by integrating only the points satisfying the conditions given by (8). Currently, there is no analytical formulation to describe fully or partially displayable points. As a result, the area of these regions is approximated by,

$$A \simeq \sum_{j=1}^{n} \sum_{k=1}^{m} \sum_{l=1}^{p} ||\mathbf{P}(r_l, \theta_k, \sigma_k)||\, \Delta r\, \Delta\theta\, \Delta\sigma \tag{10}$$

where $\mathbf{P}(r_l, \theta_k, \sigma_j)$ represents a point in the workspace satisfying the desired constraint.

To compare multiple types of manipulators with differing workspaces the area of each region must be normalized

$$\boldsymbol{\mu} = \frac{\mathbf{A}}{A_t} \tag{11}$$

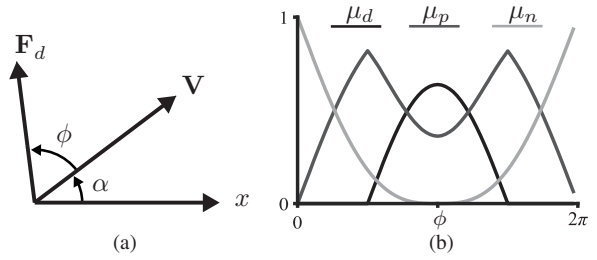

Fig. 3. The ability of a device to generate a desired force depends on the angle α and ϕ, shown in (a). The performance of serial manipulators, shown in (b), was the same for $R = 0.5, 1$, and 2, and did not vary with α.

where $\mathbf{A} = [A_d, A_p, A_n]$, with $A_t = A_d + A_p + A_n$, and the corresponding area fractions are $\boldsymbol{\mu} = [\mu_d, \mu_p, \mu_n]$. These metrics quantify the ability of a device to generate an arbitrary force for a specific input velocity direction. If the manipulator can display the desired force in all of its workspace, $\mu_d = 1$. On the other hand, $\mu_p = 1$ represents a situation where all the forces in the workspace of the device can be partially displayed. Note that $\boldsymbol{\mu}$ depends on angles $\boldsymbol{\alpha}$ and $\boldsymbol{\phi}$. Assuming $\boldsymbol{\alpha}$ is constant, one can observe the change in the displayability through the workspace of the device, as a function of the angle between velocity and the desired force along one of the components $\boldsymbol{\alpha}_a$, represented by ϕ_a, as shown in Fig. 2. Let the mean value of $\boldsymbol{\mu}$ of the three types of regions for all values of ϕ_a be

$$\boldsymbol{\eta}_a = \frac{1}{2\pi} \sum_{0}^{2\pi} \boldsymbol{\mu} \; \Delta\phi_a \tag{12}$$

where $\boldsymbol{\eta}_a = [\eta_d, \eta_p, \eta_n]$. This measure represents the ability of a device to generate any force for an arbitrary velocity. If $\eta_d = 1$, the device can generate all desired forces in all directions for the specified value of α_a. Extending this measure of displayability to all possible values of α_a yields:

$$\bar{\boldsymbol{\eta}}_a = \frac{1}{2\pi} \sum_{0}^{2\pi} \boldsymbol{\eta} \; \Delta\alpha_a \tag{13}$$

where $\bar{\boldsymbol{\eta}}_a = [\bar{\eta}_d, \bar{\eta}_p, \bar{\eta}_n]$. These metrics measure the relative percentage of the forces a haptic device can generate for all possible combinations of velocity and desired force. If $\bar{\eta}_d = 1$, the manipulator can display a desired force in any direction. These metrics can highlight the trade-offs and characteristics of each topology, thus, aiding in the design of a passive device. In this paper we analyze only planar robots, thus, $\boldsymbol{\alpha} = \alpha_a = \alpha$, $\boldsymbol{\phi} = \phi_a = \phi$, $\eta_a = \eta$ and $\bar{\eta}_a = \bar{\eta}$.

IV. Evaluating Passive Haptic Devices

The performance of serial and parallel manipulators are evaluated using metrics in (11), (12), and (13). To reduce the number of possible kinematic solutions and singularities in the workspace of the two manipulators, both manipulators were constrained to half of the reachable workspace. The analysis also assumed all parallel manipulators to be symmetric i.e., $l_1 = l_2$ and $l_3 = l_4$, with $l_5 = 0$ or 1. Link lengths of the two manipulators are normalized and only the link length ratio, $R = l_1/l_3 = l_2/l_4$ for parallel and $R = l_1/l_2$ for serial manipulators, varies. There are 3 general cases to consider for each manipulator $R = 0.5, 1, 2$. In total, 9 manipulator configurations, listed in Table I were considered.

TABLE I
The 9 configurations of serial and parallel manipulators, with their link lengths, link length ratio R, and the corresponding performance as a percentage of the workspace.

Type	R	l_1	l_2	μ_{d-max}	μ_{p-max}	$\bar{\eta}_d$	$\bar{\eta}_p$	$\bar{\eta}_n$
Serial	0.5	0.5	1	63.9	81.6	17.9	50.0	32.1
	1	1	1	63.9	81.6	17.9	50.0	32.1
	2	1	0.5	63.9	81.6	17.9	50.0	32.1
Parallel $l_5 = 0$	0.5	0.5	1	54.7	77.3	17.9	50.0	32.1
	1	1	1	63.9	81.6	17.9	50.0	32.1
	2	1	0.5	50.3	75.1	18.1	50.0	31.9
Parallel $l_5 = 1$	0.5	0.5	1	90.5	98.4	22.6	50.0	27.4
	1	1	1	62.9	92.2	18.2	50.0	31.8
	2	1	0.5	97.0	98.5	15.1	50.0	34.9

Their performance is aggregated and summarized in Table I, while the detailed results are divided into three sets. Fig. 3(b) shows the performance measures for all serial manipulators. The results for parallel manipulators are grouped by length of l_5. Fig. 4(a) and (b) shows the performance results of parallel manipulators with $l_5 = 0$. For manipulators with $l_5 = 1$, on the other hand, the performance is shown in Fig. 4(c) and (d) as well as, Fig. 5 and Fig. 6.

V. Discussion

There are clear distinctions in performance across the spectrum of manipulators. All serial manipulators performed the same, irrespective of their link length ratio R or direction of velocity α. The performance of parallel manipulators varied significantly as a function of both R and l_5. As a result, the performance of parallel manipulators will be analyzed separately for manipulators with $l_5 = 0$ and $l_5 = 1$.

A. Serial Manipulators

The results for all serial manipulators, independent of the link length ratio or the direction of velocity were the same as shown in Table I. Let $\mu_{d-max} = \max(\mu_d) \; \forall\phi, \; \forall\alpha$ represent the highest percentage of the fully displayable region μ_d. For a serial manipulator, this angle occurs when the angle between the velocity and the desired force is $\phi = \pi$, as shown in Fig. 3(b). Note that since $\mu_{d-max} < 1$, there are parts of the workspace where a force directly opposing the velocity cannot be rendered. When $\phi = \pi$, $\mu_d = 0.63$ and $\mu_p = 0.37$, which means that desired force can be generated in 63% of the device's workspace while in the remaining 37% the force can be approximated. Since $\bar{\eta}_d = \eta_d = 0.179$ and $\bar{\eta}_p = \eta_p = 0.5$, the performance of these manipulators does not vary with α. Consequently, for all combinations of α, the mean percentage of the fully and partially displayable regions in the workspace was 17.9% and 50.0% respectively. All serial manipulators, therefore, can fully or partially display 70.3% of all forces irrespective of the velocity direction.

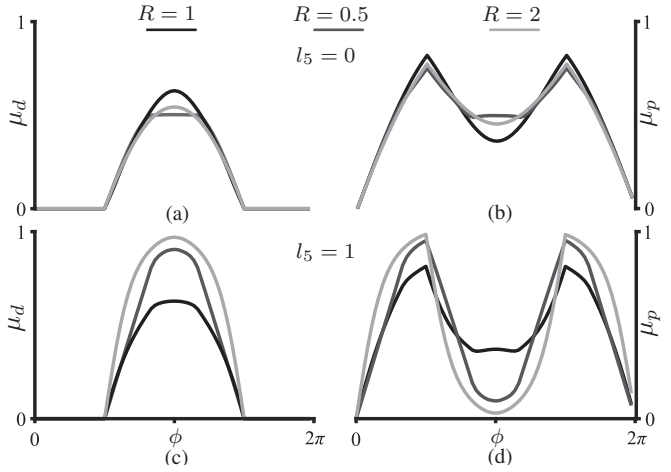

Fig. 4. Performance of the two types of parallel manipulators. Performance, μ_d and μ_p, of devices with $l_5 = 0$ for any α is shown (a) and (b), respectively. The performance of device with $l_5 = 1$, at $\alpha = \pi/2$ is shown in (c), and (d).

B. Parallel Manipulators with $l_5 = 0$

Like serial manipulators, the performance of parallel manipulators with base link length $l_5 = 0$ is insensitive to change in α, meaning that $\bar{\eta}_d = \eta_d$ and $\bar{\eta}_p = \eta_p$. Unlike serial manipulators, the performance varies depending on the link length ratio R, which is optimal when $R = 1$. Their optimal values are exactly the same as all serial manipulators, as shown in Fig. 4 (a) and (b).

Any link ratio other than $R = 1$ deteriorates μ_d, μ_p, η_d, and η_p. As shown in Table I and Fig. 4(a) and (b), the manipulator with $R = 2$ has the lowest maximum μ_d and μ_p, and the lowest $\bar{\eta}_d$ and $\bar{\eta}_p$, meaning it could generate a smaller range of forces than the manipulators with $R = 1$ or 0.5. From Fig. 4(a) and (b), the manipulator with $R = 1$ performed slightly better than manipulator with $R = 0.5$. This change is reflected in the maximum value of μ_d listed in Table I. However, the difference in η and $\bar{\eta}$ of the two manipulators is insignificant given the working precision. Thus, the link lengths of this manipulator must be equal to maximize performance, and there is no advantage to varying the link length from the perspective of a passive haptic device.

C. Parallel Manipulators with $l_5 = 1$

The performance of parallel manipulators with $l_5 = 1$ varies as a function of α and ϕ. To start, consider μ_d and μ_p of the device for $\alpha = \pi/2$, shown in Fig. 4 (c) and (d), respectively. This manipulator is much more sensitive to changes in link ratio R. The maximum fraction of the partially displayable region μ_d for the 3 manipulators varies from 0.639 to 0.97. For some velocity directions, these manipulators can create a force that opposes velocity anywhere in the workspace. The results change significantly depending on the angle α. From Fig. 6(a), the maximum value of μ_d for all angles of ϕ is shown as a function of α. Notice that at both $\alpha = 0$ and $\alpha = \pi/2$, the maximum μ_d are the same, for each of the three manipulators. This shows that at $\alpha = 0, \pi/2, \pi$, and $3\pi/2$, the manipulator with $R = 2$ can generate a force at any point

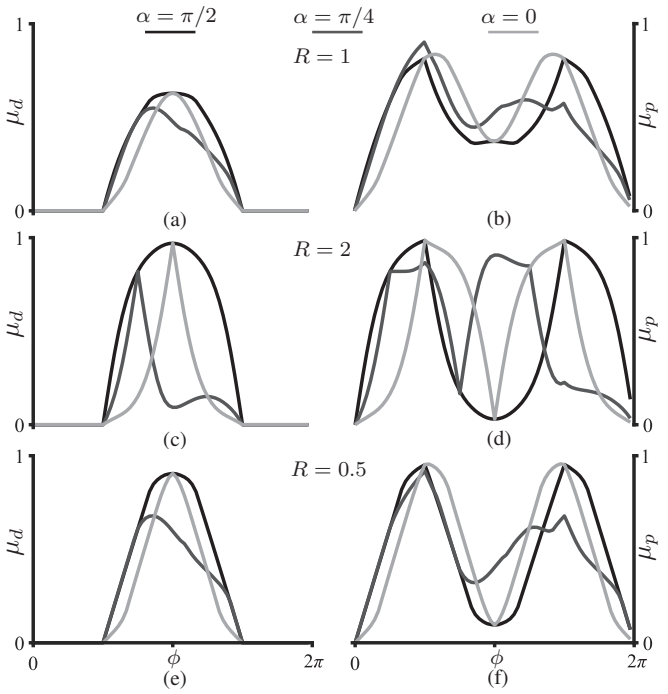

Fig. 5. Performance of parallel manipulators with $l_5 = 1$ for $\alpha = 0, \pi/4, \pi/2$. For manipulators with $R = 1$, the results are in (a) and (b), for $R = 2$ in (c) and (d), and for $R = 0.5$ in (e) and (f).

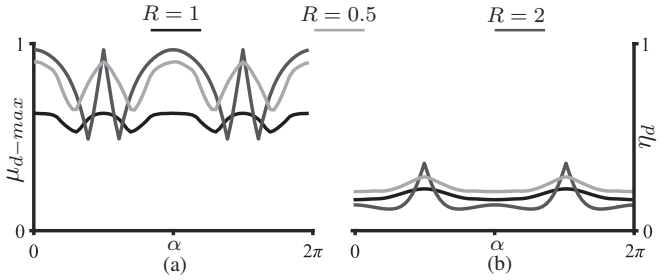

Fig. 6. The performance for parallel manipulators with $l_5 = 1$. In (a), the variation of the maximum μ_d is shown as a function of α. The variation in η_d, on the other hand, is shown in (b).

in its workspace. The peak value of μ_d for this manipulator, however, experiences the steepest drops, as shown in Fig. 6(a).

Let us focus on Fig. 6(b), which shows the variation of average fraction of the displayable region μ_d that is η_d, for the three manipulators as a function of α. Notice that, compared with Fig. 6(a), peaks of μ_d and η_d do not align. To investigate the discrepancy, let us examine Fig. 5, where μ_d and μ_p are shown for the three manipulators, at $\alpha = 0, \pi/4$, and $\pi/2$. Fig. 5(a) (c) and (e), all show that for $\alpha = 0$ and $\alpha = \pi/2$, the performance has the same peak μ_d. As the curves of μ_d and μ_p illustrate at $\alpha = \pi/2$ all 3 of the manipulators can render more forces than at $\alpha = 0$ in directions other than $\phi = \pi/2$. The peaks in Fig. 6(a) that do not correspond with peaks in (b), represent directions where force at a specific direction, can be generated almost anywhere in the workspace, but all other forces will be difficult to render.

Lastly, consider the variation in performance of the 3 manipulators, shown in Fig. 6. The performance, μ_{d-max} and

η_d, clearly varies the least in the manipulator with $R = 1$. The manipulator with $R = 2$, on the other hand, has the highest peak performances, but also steepest declines. The performance of the manipulator with $R = 0.5$ is almost as high as for the manipulator with $R = 2$, but it does not have as steep of declines i.e, $\partial\eta_d/\partial\alpha$. As a result, this manipulator performs the best, as indicated by a high value of $\bar{\eta}_d$ listed in Table I. Notice that all parallel manipulators with both manipulators with $R = 1$ and 0.5, had the highest value of $\bar{\eta}_d$ of all manipulators.

VI. Conclusions

This paper presents the first analysis of the effects of the kinematic structure on the ability of a passive haptic device to generate forces. The performance metrics introduced here evaluate the areas of the device's workspace where the desired force can be either fully displayed, or partially displayed.

The analysis considers 9 manipulators, 3 serial and 6 parallel kinematic chains, with link length ratios of 0.5, 1, and 2. The following recommendations can be made for 2-DOF RR serial and symmetric 2-DOF five-bar parallel manipulators from the findings of this paper:

- Passive serial manipulators generate forces in all directions equally well independent of the link length ratio;
- Parallel manipulators with a base link length of zero generate the widest range of forces in their workspace when all links have the same length;
- Parallel manipulators with a base link length equal to one perform better in a larger percentile of the workspace than serial manipulators;

This performance, however, varies significantly depending on the direction of the velocity. Parallel manipulators perform best when the velocity acts perpendicular to the base of the manipulator, and worst when the velocity acts at an angle of $\pi/4$ from the base link. In this category of manipulators, the one with link length ratio of 0.5, performs the best.

Serial manipulators perform equally well for all combinations of link length ratios, so no optimal configuration of this manipulator exists in terms of force displayability. For parallel manipulators there exists no global optimum solution; force displayability can only be improved for certain velocity directions. Thus, optimization of a parallel manipulator should be conducted on a case-by-case basis. During the design, the metrics presented here should be used in conjunction with other dexterity metrics to develop a fitness equation tailored to the application. These results aid in the design of 2-DOF passive haptic devices. Serial and parallel manipulators with $l_5 = 0$ are equally suitable for applications where the user is expected to move in all directions equally i.e., the most general use case. For specialized applications where the motion has a predominant direction, parallel manipulators with $l_5 > 0$ are a better choice. These applications include simulation of needle insertion tasks [25], teleoperation of robots in constrained workspaces, or upper limb patient rehabilitation [26].

The metrics proposed in this paper should be used in conjunction with other metrics, like manipulability [18], [19], dynamic capability equations [17] and workspace condition number [15], [16], to design a passive haptic device with the desired force output capability and dynamic characteristics.

References

[1] J. E. Colgate and G. G. Schenkel, "Passivity of a class of sampled-data systems: Application to haptic interfaces," *J. of Robotic Sys.*, vol. 14, no. 1, pp. 37–47, 1997.

[2] J. An and D.-S. Kwon, "Five-bar linkage haptic device with DC motors and MR brakes," *J. of Intell. Mater. Syst. and Struct.*, vol. 20, no. 1, pp. 97–107, 2009.

[3] V. Hayward and K. E. MacLean, "Do it yourself haptics: part I," *IEEE Robotics & Automat. Mag.*, vol. 14, no. 4, 2007.

[4] W. J. Book *et al.*, "The concept and implementation of a passive trajectory enhancing robot," in *Intell. Machine Dyn. Lab. Publications*. Georgia Institute of Technology, 1996.

[5] C. Rossa, J. Lozada, and A. Micaelli, "Design and control of a dual unidirectional brake hybrid actuation system for haptic devices," *IEEE Trans. Haptics*, vol. 7, no. 4, pp. 442–453, 2014.

[6] M. R. Reed and W. J. Book, "Modeling and control of an improved dissipative passive haptic display," in *Proc. of IEEE Int. Conf. on Robotics and Automat.*, vol. 1. IEEE, 2004, pp. 311–318.

[7] B. Kent, A. Cusipag, and C. Rossa, "Tissue discrimination through force-feedback from impedance spectroscopy in robot-assisted surgery," in *Int. Conf. on Smart Multimedia, 2019*, Dec 2019.

[8] A. Bicchi and G. Tonietti, "Fast and "soft-arm" tactics," *IEEE Robotics & Automat Mag.*, vol. 11, no. 2, pp. 22–33, 2004.

[9] H. Davis and W. Book, "Torque control of a redundantly actuated passive manipulator," in *Proc. of the 1997 Amer. Control Conf.*, vol. 2. IEEE, 1997, pp. 959–963.

[10] C. Cho, M. Kim, and J.-B. Song, "Direct control of a passive haptic device based on passive force manipulability ellipsoid analysis," *Int. J. of Control, Automat., and Syst.*, vol. 2, no. 2, pp. 238–246, 2004.

[11] C. Cho, J.-B. Song, and M. Kim, "Energy-based control of a haptic device using brakes," *IEEE Trans. Syst., Man, Cybern. Syst.*, vol. 37, no. 2, pp. 341–349, 2007.

[12] D. Karnopp, "Computer simulation of stick-slip friction in mechanical dynamic systems," *J. of Dynamic Syst., Meas., and control*, vol. 107, no. 1, pp. 100–103, 1985.

[13] M. Łącki and C. Rossa, "On the feasibility of multi-degree-of-freedom haptic devices using passive actuators," in *IEEE Int. Conf. on Intell. Robots and Syst.*, Nov 2019, pp. 7282–7287.

[14] S. Briot and I. A. Bonev, "Are parallel robots more accurate than serial robots?" *Trans. of the Can. Soc. for Mech. Eng.*, vol. 31, no. 4, pp. 445–455, 2007.

[15] C. M. Gosselin, "Dexterity indices for planar and spatial robotic manipulators," in *Proc., IEEE Int. Conf. on Robotics and Automat.* IEEE, 1990, pp. 650–655.

[16] C. Gosselin and J. Angeles, "A global performance index for the kinematic optimization of robotic manipulators," *J. of Mech. Des.*, vol. 113, no. 3, pp. 220–226, 1991.

[17] A. Bowling and O. Khatib, "The dynamic capability equations: a new tool for analyzing robotic manipulator performance," *IEEE Trans. Robot.*, vol. 21, no. 1, pp. 115–123, 2005.

[18] H. Asada, "A geometrical representation of manipulator dynamics and its application to arm design," *J. of Dyn. Syst., Meas., and Control*, vol. 105, no. 3, pp. 131–142, 1983.

[19] A. Bicchi and D. Prattichizzo, "Manipulability of cooperating robots with unactuated joints and closed-chain mechanisms," *IEEE Trans. Robot. Autom.*, vol. 16, no. 4, pp. 336–345, 2000.

[20] S. L. Chiu, "Task compatibility of manipulator postures," *The Int. J. of Robotics Res.*, vol. 7, no. 5, pp. 13–21, 1988.

[21] C. Cho, J.-B. Song, and M. Kim, "Design and control of a planar haptic device with passive actuators based on passive force manipulability ellipsoid analysis," *J. of Robotic Syst.*, vol. 22, no. 9, pp. 475–486, 2005.

[22] G. T. Pond and J. A. Carretero, "Quantitative dexterous workspace comparison of serial and parallel planar mechanisms," in *Parallel Manipulators, New Developments*. IntechOpen, 2008.

[23] S. Cubero, *Industrial robotics: Theory, modelling and control*. Pro Literatur Verlag, 2006.

[24] X.-J. Liu, J. Wang, and G. Pritschow, "Kinematics, singularity and workspace of planar 5r symmetrical parallel mechanisms," *Mechanism and Machine Theory*, vol. 41, no. 2, pp. 145–169, 2006.

[25] C. Rossa and M. Tavakoli, "Issues in closed-loop needle steering," *Control Eng. Pract.*, vol. 62, pp. 55–69, 2017.

[26] B. DeBoon *et al.*, "Differentially-clutched series elastic actuator for robot-aided musculoskeletal rehabilitation," in *Int. Conf. on Robotics and Automat. (ICRA)*. IEEE, 2019, pp. 1507–1513.